RSC Advances

PAPER

View Article Online
View Journal | View Issue

Cite this: *RSC Adv.*, 2025, **15**, 28659

Enhanced catalytic performance of transition metal-doped Co/TiO_2 for continuous-flow synthesis of borneol from isoborneol

Chenyang Li,†[a] Zhihan Liu,†[a] Huimin Li,[b] Yunsen Xiao,[b] Ying Huang,[a] Yuting Lin,[a] Jie Liu,[a] Bin Wu,[b] Fuweng Zhang,[b] Huidong Zheng *[ab] and Longfei Yan *[b]

Received 27th May 2025
Accepted 6th August 2025

DOI: 10.1039/d5ra03723a

rsc.li/rsc-advances

Borneol, a pharmaceutically important monoterpenoid, has emerged as a key ingredient in modern medicinal formulations. Here, we report a highly efficient heterogeneous catalytic system using transition metal-doped Co/TiO_2 catalysts for the continuous-flow isomerization of isoborneol to borneol. Through systematic screening of bimetallic combinations, we demonstrate that Cu and Ni dopants synergistically enhance the redox properties of Co species, particularly improving hydrogenation–dehydrogenation efficiency in the isomerization of isoborneol. The optimized 1Cu–3Co/TiO_2 catalyst (Cu : Co = 1 : 3 mass ratio) enabled a two-stage continuous-flow system, achieving 58% molar yield of borneol with <0.4% camphor byproduct formation after solvent removal. Remarkably, the catalyst maintained >99% metal retention during a total of 200 h of continuous reaction. This work not only provides fundamental insights into promoter effects in bimetallic catalysis but also establishes a commercially viable platform for continuous production of high-purity botanical therapeutics.

1 Introduction

Borneol ($C_{10}H_{18}O$), a bicyclic monoterpenoid alcohol, is a pharmacologically active compound with wide applications in both pharmaceutical and cosmetic industries.[1–3] Commercially available borneol exists in two distinct grades: natural and synthetic. Natural borneol, extracted from the endangered "*Dryobalanops aromatica* tree", has limited availability and commands premium pricing, making it exclusively suitable for high-end medicinal formulations.[4,5] In contrast, synthetic borneol, synthesized from turpentine *via* catalytic isomerization, constitutes over 90% of the commercial market owing to its cost-effectiveness and industrial scalability.[6] Notably, the Chinese Pharmacopoeia (ChP) sets a minimum purity requirement of 55% for medicinal borneol, creating substantial opportunities for catalytic process innovation to improve production efficiency and product quality.[7]

The synthesis of borneol predominantly employs α-pinene, a major turpentine derivative, as the feedstock.[8] However, conventional synthetic routes typically yield a low-value isoborneol as an undesired by-product.[9] This not only increases the cost of purification but also compromises the final product quality.[10,11] Catalytic isomerization of isoborneol to borneol presents a promising strategy to both enhance the economic value of the isoborneol and upgrade the quality of borneol. Notably, the isomerization process involves competing reaction pathways, including dehydrogenation to camphor and dehydration to camphene,[12] as shown in Fig. 1. According to the ChP, synthetic borneol must contain less than 0.5% camphor.[13] Therefore, the design of highly selective bifunctional catalysts is critical to facilitate isoborneol isomerization and suppress camphor formation.[14]

Our previous work demonstrated a one-pot, two-step catalytic system employing $NaBH_4$-reduced Co/TiO_2 catalysts, achieving 62.3% borneol yield.[15,16] However, this system relied on $NaBH_4$-mediated size control of metallic Co nanoparticles, which presents scalability challenges for industrial production. Furthermore, the batch-type reaction limits large-scale borneol

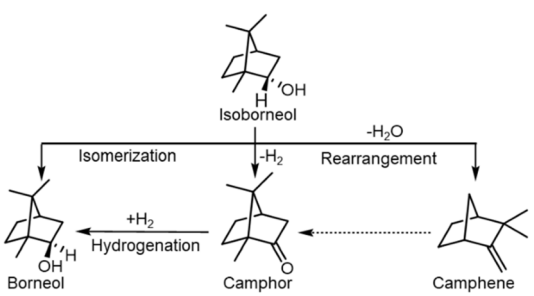

Fig. 1 Reaction mechanism of isoborneol isomerization.

[a]*Fujian Engineering Research Center of Advanced Manufacturing Technology for Fine Chemicals, College of Chemical Engineering, Fuzhou University, Fuzhou, Fujian, 350108, PR China. E-mail: youngman@fzu.edu.cn*

[b]*Qingyuan Innovation Laboratory, Quanzhou, Fujian, 362801, PR China. E-mail: yan_lf.qyil@qq.com*

† Chenyang Li and Zhihan Liu contributed equally to this work.

synthesis. Herein, we report a two-stage continuous-flow system using a H_2-activated bimetallic M-Co/TiO_2 (M = Cu, Ni) catalysts to address both challenges. Transition metal doping significantly facilitates the catalysts' reduction properties while maintaining high stereoselectivity. The optimized system achieves 58% yield of borneol in continuous-flow reaction, with camphor byproduct controlled below 0.4%, which meets the requirements of the ChP.

2 Experimental

2.1 Materials

$Co(NO_3)_2 \cdot 6H_2O$ (99%), $Cu(NO_3)_2 \cdot 3H_2O$ (99%), $Ni(NO_3)_2 \cdot 6H_2O$ (99%), $Fe(NO_3)_3 \cdot 9H_2O$ (99%) and $ZnCl_2$ (99.99%) were purchased from Aladdin. TiO_2 (99.99%), isoborneol (97%), camphor (98%) and heptane (99%) were purchased from Adamas. All reagents were used without further purification.

2.2 Preparation of M-Co/TiO_2 catalysts

0.96 g TiO_2 and 0.15 g $Co(NO_3)_2 \cdot 6H_2O$ were added to a 100 mL beaker containing 20 mL deionized water. The mixture was vigorously stirred for 3 h, then evaporated at 80 °C with stirring to dryness. The solid was vacuum-dried at 60 °C for 12 h, followed by reduction under 5 vol% H_2/N_2 flow (10 mL min^{-1}) by heating to 500 °C at 3 °C min^{-1} and holding for 2 h, and then passivated under 1 vol% O_2/N_2 flow (10 mL min^{-1}) at room temperature for 12 h. The resulting catalyst denoted as 3Co/TiO_2 (3 wt% Co).

For bimetallic catalysts, 3Co/TiO_2 was used as the support. Specifically, 0.99 g of 3Co/TiO_2 and 0.04 g $Cu(NO_3)_2 \cdot 3H_2O$ (1 wt% Cu) were dispersed in 20 mL deionized water. After stirring for 3 h, the mixture was dried and reduced under the same conditions as those used for 3Co/TiO_2, the catalyst was denoted as 1Cu–3Co/TiO_2 (the number before each metal represents the metal's mass loading, *e.g.*, 1 wt% Cu, 3 wt% Co). Analogously, Ni–Co/TiO_2, Fe–Co/TiO_2, Zn–Co/TiO_2 were prepared by replacing $Cu(NO_3)_2 \cdot 3H_2O$ with $Ni(NO_3)_2 \cdot 6H_2O$, $Fe(NO_3)_3 \cdot 9H_2O$, or $ZnCl_2$, respectively. The 1Co–3Co/TiO_2 catalyst was also prepared using the same method as the bimetallic catalyst. The oxidized variant (1CuO_x–3CoO_x/TiO_2) was obtained through calcination in air instead of H_2 reduction.

2.3 Characterizations

Powder X-ray diffraction (XRD) patterns were recorded on a Panalytical X'Pert3 diffractometer. Hydrogen temperature-programmed reduction (H_2-TPR) measurements were performed using a BELCAT II chemisorption analyser. Metal loadings were determined by inductively coupled plasma mass spectrometer (ICP-MS). Transmission electron microscopy (TEM), high-angle annular dark-field scanning transmission electron microscopy (HAADF-STEM), and energy-dispersive spectroscopy (EDS) elemental mapping measurements were performed on a JEM-F200 electron microscope. X-ray photoelectron spectroscopy (XPS) measurements were performed on a ESCALAB QXi (Thermo Scientific) using Al Kα radiation (1846.6 eV) as the X-ray source. N_2 adsorption–desorption measurements were conducted using a Micromeritics ASAP 2460 automated sorption system. More detailed characterizations are provided in SI.

2.4 Catalyst evaluation

2.4.1 Isomerization of isoborneol in a batch reactor. A 100 mL stainless steel autoclave (Shanghai LABE Instrument Co., Ltd) was charged with the catalyst (0.25 g), heptane (30 mL) and isoborneol (0.50 g). The reactor was purged five times with H_2 at 0.5 MPa, then pressurized to 3.0 MPa with H_2. The mixture was stirred at 500 rpm while heating to 160 °C. After the reaction was complete, the reactor was cooled to room temperature.

2.4.2 Isomerization of isoborneol in a continuous flow reactor. The continuous isomerization of isoborneol to borneol was performed in a continuous-flow reactor (Oushisheng, H-Flow-S50), as shown in Fig. S1. The reaction tube was a stainless steel pipe (500 mm length, 20 mm inner diameter) equipped with an oil-heating jacket. Additional design and experiment are provided in the SI.

2.4.3 Products analysis. The reaction mixture was filtered through a 0.22 μm syringe filter to remove the solid catalyst, and the filtrate was analyzed by gas chromatography (GC). Product identification was performed using gas chromatography-mass spectrometry (GC-MS), the corresponding spectra are provided in Fig. S2 and S3. The detailed analysis method is described in the SI. The isoborneol conversion, product yield, and Weight Hourly Space Velocity (WHSV) were calculated as follows:

$$\text{Isoborneol conversion (\%)} = (n_{iso,0} - n_{iso,1})/n_{iso,0} \times 100\% \quad (1)$$

$$\text{Products yield (\%)} = n_i/n_{iso,0} \times 100\% \quad (2)$$

$$\text{WHSV } (h^{-1}) = q_{iso}/m_c \quad (3)$$

where $n_{iso,0}$ and $n_{iso,1}$ are the molar amounts of isoborneol before and after the reaction, respectively; n_i is the molar amount of the product; q_{iso} is the mass flow rate of isoborneol; m_c is the mass of catalyst.

3 Results and discussions

3.1 The influence of the metal active sites on the isomerization of isoborneol

This work systematically investigated the catalytic performance of transition metals (Cu, Co, Ni) supported on TiO_2 for isoborneol isomerization, and the XRD patterns are shown in Fig. S4. As summarized in Table 1, the Co/TiO_2 catalyst afforded a borneol yield of >46%, whereas Cu/TiO_2 and Ni/TiO_2 yielded less than 10% under identical reaction conditions. The Cu/TiO_2 catalyst predominantly generated dehydrogenated products (camphor), with borneol yields below 1%. Notably, camphene formation was undetectable across all tested catalytic systems. These results suggest that Co species likely serve as the most effective active sites for isomerization of isoborneol.[17–19]

Table 1 The catalytic performance of catalysts with different metal active sites[a]

Catalyst	Isoborneol conversion (%)	Yield (%)		
		Camphor	Camphene	Borneol
5Co/TiO_2	65.45	18.67	0.00	46.41
5Cu/TiO_2	13.83	13.34	0.00	0.86
5Ni/TiO_2	32.35	22.86	0.00	9.83

[a] Reaction conditions: 0.25 g catalyst, 3 MPa H_2, 160 °C, 30 mL heptane, 0.5 g isoborneol, 2 h.

3.2 Effect of metal loading on catalytic performance of Co/TiO_2 catalysts

Building upon these findings, we systematically evaluated a series of Co/TiO_2 catalysts with varying cobalt loadings (1–5 wt%) for isoborneol isomerization, as shown in Fig. 2(a). The catalytic performance exhibited a distinct cobalt-loading dependence, with borneol yield increasing linearly from 9.7% to 46.4% as Co loading rose from 1 to 5 wt%. However, the 5 wt% Co/TiO_2 catalyst still generated considerable camphor byproduct (18.7%). To enhance hydrogenation activity while maintaining cost efficiency, we introduced secondary transition metals (Cu, Ni, Zn, Fe) into 3 wt% Co/TiO_2, as shown in Fig. 2(b). Notably, Cu and Ni doping significantly improved the borneol yield (51.4% and 51.9%, respectively) while simultaneously suppressing camphor formation to 11.7%. In contrast, Zn and Fe incorporation caused catalyst deactivation. Further optimization of Cu–Co/TiO_2 revealed that increasing Co loading from 1 wt% to 3 wt% significantly improved the borneol yield, as shown in Fig. 2(c). The 1Cu–3Co/TiO_2 catalyst achieved a borneol yield of 51.4%, whereas 1Cu–4Co/TiO_2 showed a slight increase to 52.2%, with negligible change in camphor yield (<1%). Considering the balance between catalytic activity and economic efficiency, 1Cu–3Co/TiO_2 was selected as the optimal catalyst.

H_2-TPR characterization was performed to elucidate the effect of secondary metals on the reducibility of bimetallic catalysts, as shown in Fig. 2(d). The 1Zn–3Co/TiO_2 catalyst displayed a prominent reduction peak at 341 °C, closely resembling that of 3Co/TiO_2, suggesting that Zn incorporation exerts minimal effects on Co reducibility. In contrast, 1Fe–3Co/TiO_2 exhibited a broad peak shifted to ~400 °C compared to 3Co/TiO_2, corresponding to the FeO → Fe^0 reduction process. The disappearance of the original Co peak at 334 °C suggested synergistic Co–Fe reduction at 400 °C, which increased the reduction activation energy and consequently decreased catalytic activity. The H_2-TPR profile of the 1Ni–3Co/TiO_2 catalyst featured two distinct reduction peaks at 304 °C and 380 °C, attributed to the reduction of CoO_x and NiO_x, respectively. Meanwhile, the 1Cu–3Co/TiO_2 catalyst demonstrated a significantly lower reduction temperature at 231 °C. These results indicate that both Ni and Cu facilitate the reduction of Co, likely because their doping enhances the dispersion of Co on the TiO_2 support. Thereby improving the isomerization of isoborneol and hydrogenation of camphor.[20–22] HAADF-STEM and EDS elemental mapping showed that the 3Co/TiO_2 catalyst contained large and agglomerated Co particles (~14 nm), as shown in Fig. 3(a) and S5. Cu doping into 3Co/TiO_2 significantly reduced the Co nanoparticle size to ~12 nm, as shown in Fig. 3(b), (c) and S5. Moreover, in 1Cu–3Co/TiO_2, Cu was in close contact with Co nanoparticles, and the Co distribution became more dispersed, as shown in Fig. 3(d)–(f). These results can be attributed to the high dispersibility of Cu on the support surface, which in turn enhanced the dispersion of Co on TiO_2.[23] The Cu–Co interaction likely further improved the reducibility of the catalyst upon Cu doping (Fig. 2(d)).

3.3 The recyclability of the 1Cu–3Co/TiO_2 catalyst

The recyclability of heterogeneous catalysts is crucial for cost-effective and sustainable chemical processes. Therefore, the

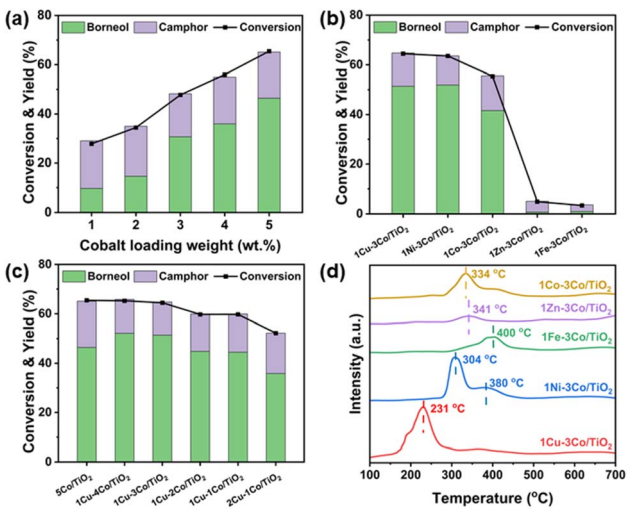

Fig. 2 The effects of metal loading for catalytic performance. (a) The influence of Co-loading weight, (b) the influence of secondary transition metals, (c) the influence of different ratio of Cu/Co, (d) H_2-TPR of M-3Co/TiO_2 catalysts. Reaction conditions: 0.25 g catalyst, 3 MPa H_2, 160 °C, 30 mL heptane, 0.5 g isoborneol, 2 h.

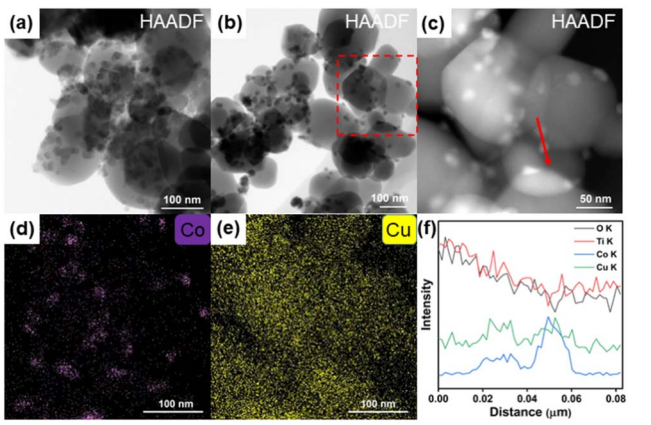

Fig. 3 TEM characterizations of 3Co/TiO_2 and 1Cu–3Co/TiO_2. (a) HAADF-STEM image of Co/TiO_2. (b and c) HAADF-STEM image of 1Cu–3Co/TiO_2. (d and e) EDS mapping patterns of Co and Cu over 1Cu–3Co/TiO_2. (f) Line-scanning elemental distribution for 1Cu–3Co/TiO_2 along the red arrow in (c).

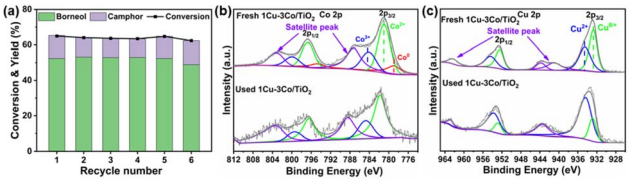

Fig. 4 The recyclability of the 1Cu–3Co/TiO_2 catalyst. (a) Catalytic performance, (b) Co 2p and (c) Cu 2p XPS spectra of 1Cu–3Co/TiO_2 before and after reaction. Reaction conditions: 0.25 g catalyst, 3 MPa H_2, 160 °C, 30 mL heptane, 0.5 g isoborneol, 2 h.

stability of the bimetallic 1Cu–3Co/TiO_2 catalyst was evaluated in the isomerization of isoborneol to borneol, as shown in Fig. 4(a). In the recycling tests, each reaction cycle was run for 2 hours. The catalyst was then filtered, washed, and vacuum-dried for reuse. The catalyst demonstrated excellent stability during the initial five reaction cycles, maintaining a consistent borneol yield of 52.0%, while camphor formation exhibited only a marginal increase from 10.2% to 12.4%. However, a notable decline in catalytic performance occurred in the sixth cycle, with borneol yield dropping to 48.9% and camphor yield rising to 13.5%. BET analysis of 1Cu–3Co/TiO_2 before and after reaction revealed no significant changes in specific surface area and pore structure distribution (Fig. S6 and Table S1). In contrast, the characteristic diffraction peak at 44.3°, assigned to the (002) plane of metallic Co,[24,25] exhibited significant attenuation after cycling (Fig. S7), this is likely due to oxidation of metallic Co species on the catalyst surface. XPS analysis further supported this observation, and the results showed that the oxidized Co species (Co^{2+}) increased significantly from 57.1% to 73.0% after the reaction, with the complete disappearance of Co^0, as shown in Fig. 4(b) and Table S2. Combined with the observed decline in isomerization activity (Fig. 4(a)), these findings suggest that the oxidation of surface metallic Co during the reaction may deactivate the active sites, leading to reduced catalytic performance.

3.4 Continuous catalytic isomerization of isoborneol to borneol over a 1Cu–3Co/TiO_2 catalyst

While the 1Cu–3Co/TiO_2 catalyst exhibits high activity for the isomerization of isoborneol to borneol in a batch reactor, its practical application faces limitations due to oxidative deactivation and low production efficiency. As illustrated in Fig. S1, a two-stage continuous flow system for borneol synthesis was designed to overcome these limitations. This system not only enhances production efficiency but also prevents catalyst exposure to air, thereby enhancing long-term stability by suppressing cobalt oxidation.

The two-stage continuous-flow system first isomerizes isoborneol to yield a borneol-rich mixture containing camphor, followed by hydrogenation of camphor in the second-stage to improve product quality. Systematic parameter optimization was performed in this system for borneol synthesis. In the isomerization reaction, increasing temperature promoted both target and side reactions: borneol yield increased from 46.7% to

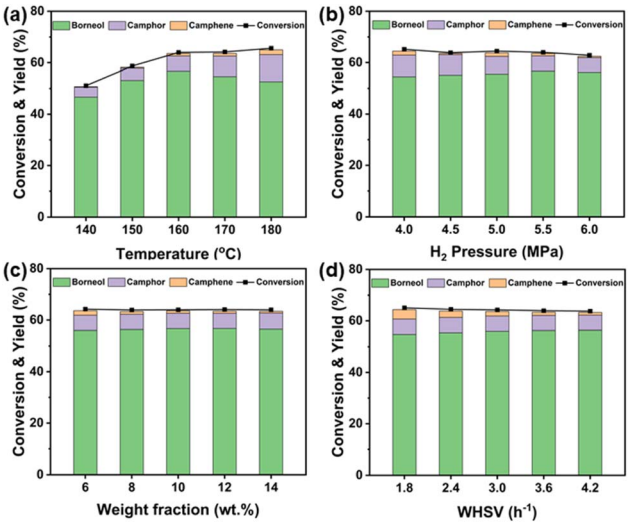

Fig. 5 The effects of reaction conditions in the isomerization stage. (a) Reaction temperatures, (b) reaction pressure, (c) substrate concentration, (d) WHSV. General reaction conditions: 160 °C, 5.5 MPa of 50 mL per min H_2, 4.2 per h WHSV, 25.5 g catalyst, and 10 wt% isoborneol.

52.6%, while camphor formation rose from 3.9% to 10.6%, as shown in Fig. 5(a). While system pressure had minimal impact on borneol yield, it significantly suppressed camphor formation (from 8.4% at 4.0 MPa to 5.7% at 6.0 MPa, Fig. 5(b)). In comparison, substrate concentration and WHSV showed slight effects on product distribution, as shown in Fig. 5(c) and (d). After comprehensive consideration of both catalytic performance and process safety, the optimal conditions were determined to be 160 °C, 5.5 MPa of H_2, 4.2 per h WHSV, and 10 wt% isoborneol concentration, achieving 56.7% borneol yield with 5.9% camphor byproduct.

During the isomerization of isoborneol under optimized conditions, the borneol yield reached >55%, but the camphor content (5.9%) significantly exceeded the ChP limit of 0.5% for medicinal borneol. To comply with the standard, further hydrogenation of camphor was necessary, as shown in Fig. 6. In the hydrogenation reaction, the product mixture (composition: borneol 55.6%, camphor 5.4%, camphene 0.6%) obtained from the isomerization reaction was used as the feedstock (denoted as R_0). As shown in Fig. 7(a), low temperature favored the hydrogenation of camphor to isoborneol, whereas high temperature promoted borneol formation but reduced camphor conversion. Pressure studies demonstrated that although lower pressures (4.0–4.5 MPa) maximized borneol content, the camphor content (0.57–0.62%) exceeded the ChP standards

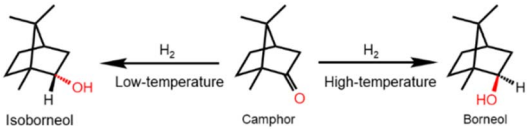

Fig. 6 Selective hydrogenation of camphor at different temperature.

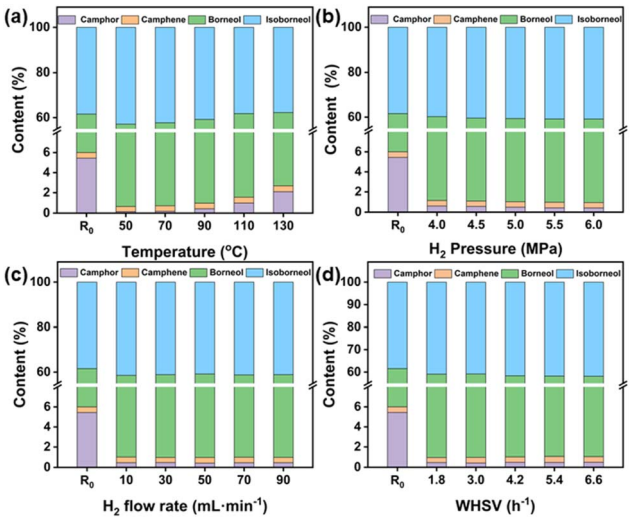

Fig. 7 The effects of reaction conditions in the hydrogenation stage. (a) Reaction temperatures, (b) reaction pressure, (c) H_2 flow rate, (d) WHSV. R_0: the reaction products mixture from the isomerization reaction. General reaction conditions: 90 °C, 5.5 MPa of 50 mL per min H_2, 3.0 per h WHSV, and 25.5 g catalyst.

(<0.5%), as shown in Fig. 7(b). At H_2 flow rates of 10–90 mL min^{-1}, camphor content was effectively reduced, as shown in Fig. 7(c). At a relatively low WHSV (1.8–3.0 h^{-1}), both borneol and camphor contents complied with ChP standards, as shown in Fig. 7(d). Based on these results, the optimal hydrogenation conditions were determined to be 90 °C, 5.5 MPa, 50 mL per min H_2 flow rate, and 3.0 per h WHSV.

3.5 The active sites for isomerization and hydrogenation

The results in Table 1 demonstrate that Co species are more effective than Cu and Ni for isoborneol isomerization. To identify whether the active site is Co^0 or Co^{2+}, unreduced $1CuO_x$–$3CoO_x/TiO_2$ was employed to catalyze the isomerization of isoborneol and the hydrogenation of camphor in a batch reactor. As summarized in Table S3, this catalyst only achieved a 23.6% borneol yield. XPS analysis revealed that 16.6% of Co^0 is present in the 1Cu–3Co/TiO_2 catalyst, whereas no Co^0 was detected in $1CuO_x$–$3CoO_x/TiO_2$, as shown in Fig. 8 and Table S2. This difference in Co^0 content may explain the enhanced catalytic performance of 1Cu–3Co/TiO_2. Further evaluation of camphor hydrogenation revealed that 1Cu–3Co/TiO_2 significantly outperformed single-metal catalysts (1Cu/TiO_2 and 3Co/TiO_2) and the unreduced $1CuO_x$–$3CoO_x/TiO_2$ catalyst. Notably, the 3Co/TiO_2 exhibited weak activity, whereas the 1Cu/TiO_2 and $1CuO_x$–$3CoO_x/TiO_2$ were inactive under the tested conditions (Table S3). These results indicate that both Co^0 and Co^{2+} can catalyze the isomerization of isoborneol. However, Co^0 exhibits significantly higher catalytic activity than Co^{2+}, establishing it as the predominant active site. Furthermore, the hydrogenation of camphor occurs exclusively on the surface of Co^0. Cu doping enhances the dispersion of Co on TiO_2, thereby improving catalytic efficiency in both reactions (Fig. 3).

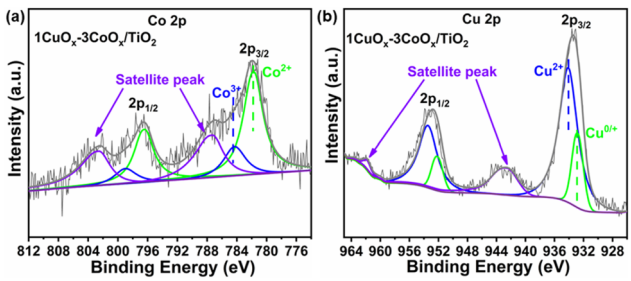

Fig. 8 XPS spectra of $1CuO_x$–$3CoO_x/TiO_2$. (a) Cu 2p, (b) Co 2p.

3.6 The long-term stability of the 1Cu–3Co/TiO_2 in the two-stage continuous flow reactor

Building upon the optimized reaction conditions established for high-temperature isomerization (160 °C, 5.5 MPa) and low-temperature hydrogenation (90 °C, 5.5 MPa), we systematically evaluated the long-term stability of the 1Cu–3Co/TiO_2 catalyst in isomerization and hydrogenation reactions, as shown in Fig. 9. The catalyst exhibited exceptional performance during 100 h continuous isomerization, maintaining stable borneol yields exceeding 55.0% while effectively controlling camphor formation at 5.5%. Subsequent direct utilization of the isomerization products in the hydrogenation stage revealed remarkable catalytic durability, with borneol content showing only a minimal decrease from 58.3% to 56.8% over 100 h of reaction, while camphor content remained <0.5%. This integrated process successfully synthesized high-quality borneol, with borneol content >57% and camphor content below 0.5%, fully complying with the ChP standards. ICP-MS analysis revealed minimal metal leaching (Co loss: 1.75 wt%; Cu loss:

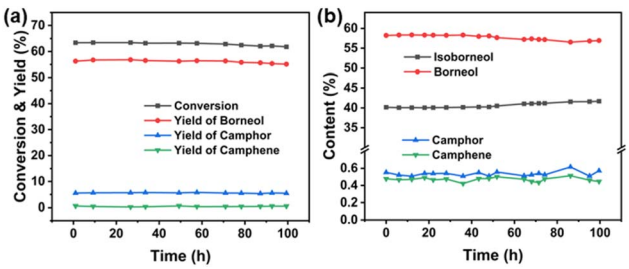

Fig. 9 Stability test of 1Cu–3Co/TiO_2 in the two stage reaction. (a) Isomerization stage, (b) hydrogenation stage. Reaction conditions: 5.5 MPa of 50 mL per min H_2, 25.5 g catalyst, and 10 wt% isoborneol, 160 °C, 3.0 per h WHSV for isomerization and 90 °C, 2.4 per h WHSV for hydrogenation (To avoid pipeline blockage from borneol precipitation in heptane under low-temperature conditions, the WHSV was maintained at 2.4 h^{-1}).

Table 2 Loadings of Co and Cu in the 1Cu–3Co/TiO_2 bimetallic catalyst before and after reaction

	Elemental content (wt%)	
Catalyst	Co	Cu
Fresh 1Cu–3Co/TiO_2	3.0737	1.0595
Used 1Cu–3Co/TiO_2	3.0199	1.0083

Table 3 Composition analysis of products before and after purification[a]

	Content (%)				
Sample	*n*-Hep.	CPE	CPO	Isobor.	Bor.
Crude product	—	0.52	0.48	40.59	57.09
Purified product	0.52	0.15	0.35	39.93	57.94
Solvent	99.80	0.03	0.005	0.09	0.07

[a] *n*-Hep.: *n*-heptane; CPE: camphene; CPO: camphor; isobor.: isoborneol; bor.: borneol.

Table 4 Residual Co and Cu content in solvents and products after purification

	Elemental content (ppm)	
Sample	Co	Cu
Recovered solvent	100	100
Purified product	200	<100

4.83 wt%, relative to initial loading, Table 2) after 200 h of total reaction, confirming outstanding structural stability.

3.7 The purification of the crude borneol products

The crude borneol products were purified through vacuum rotary evaporation (40 °C, 2 kPa) to remove residual solvents, followed by gas chromatographic (GC) analysis to determine the purity of both the recovered solvents and crystalline products. As summarized in Table 3, the final product exhibited high purity, with a composition of 57.9% borneol and 0.35% camphor, fully meeting the purity requirements of the ChP. Notably, ICP-MS analysis detected minimal metal leaching in both the recovered solvents (Co < 100 ppm, Cu < 100 ppm) and purified borneol product (Co < 200 ppm, Cu < 100 ppm), as shown in Table 4. These results demonstrate not only the exceptional stability of the 1Cu–3Co/TiO_2 catalyst under prolonged reaction conditions but also the absence of significant metal contamination in the product, suggesting its potential for high-quality borneol synthesis.

4 Conclusions

This work demonstrates an efficient continuous process for high-quality borneol production through tandem high- and low-temperature catalytic stages. Using a bimetallic 1Cu–3Co/TiO_2 catalyst in a two-stage continuous-flow system, the final product (after solvent removal) contained 58.0% borneol with <0.4% camphor, fully complying with ChP standards. The research revealed that Cu and Ni dopants significantly facilitated the reduction of surface Co species, thereby enhancing catalytic activity. In contrast, Fe and Zn dopants formed surface layers that physically blocked Co active sites and reduced performance. Under optimized conditions, the 1Cu–3Co/TiO_2 catalyst maintained stable activity for at least 200 h, demonstrating its potential for continuous isoborneol upgrading in industrial applications.

Author contributions

This manuscript was written with contributions from all authors. Chenyang Li and Zhihan Liu: data curation, formal analysis, investigation, and writing – original draft. Huimin Li, Yuanseng Xiao, Ying Huang and Yuting Liu: data curation. Jie Liu and Bin Wu: visualization. Fuweng Zhang: writing – review & editing. Huidong Zheng: resources and project administration. Longfei Yan: conceptualization, funding acquisition, methodology and writing – review & editing.

Conflicts of interest

There are no conflicts to declare.

Data availability

All data generated or analyzed during this study are included in this manuscript and the SI. The datasets used and/or analyzed during the current study are available from the corresponding author on reasonable request. Data are openly available in a public repository.

Additional details supporting the findings of this study are available in the SI. See DOI: **https://doi.org/10.1039/d5ra03723a**.

Acknowledgements

This work was supported by the Quanzhou City Science and Technology Program (No.2024QZC006R), The Starting Research Fund of Qingyuan Innovation Laboratory (No. 00522004), The Quangang Science and Technology Program Project (No. 2023KT05).

Notes and references

1 N. I. Tracy, D. Chen, D. W. Crunkleton and G. L. Price, *Fuel*, 2009, **88**, 2238–2240.
2 H. Cheng, M. Liang, S. Dai, X. Lu, Q. Huang, F. Lai, L. Ma, W. Li, X. Liu and A. J. of, *Chem*, 2023, **16**, 105322.
3 Y. Yang, X. Xu, H. He, D. Huo, X. Li, L. Dai and C. Si, *Int. J. Biol. Macromol.*, 2023, **242**, 124773.
4 Z. Lu, Z. Ma, M. Fu and J. Su, *Biochem. Genet.*, 2025, **63**, 1310–1329.
5 Q. L. Zhang, B. M. Fu and Z. J. Zhang, *Drug Delivery*, 2017, **24**, 1037–1044.
6 J. E. Sánchez-Velandia, E. Pájaro, A. L. Villa and F. Martínez-O, *Microporous Mesoporous Mater.*, 2021, **324**, 111273.
7 R. Ma, D. Lu, J. Wang, Q. Xie and J. Guo, *Biomed. Pharmacother.*, 2023, **164**, 114668.
8 H. Wang, L. H. Jiang, Y. M. Wang, Y. N. Zheng, X. X. Jiao and D. Pan, *Inorg. Nano-Met. Chem.*, 2018, **48**, 23–30.
9 S. V. Bhat, M. O. Gupta and K. R. Vaze, *Org. Prep. Proced. Int.*, 2024, **56**, 99–104.

10 M. Y. Lu, Y. Xie, H. Huang, Y. L. Zhao, H. T. An, X. Zhang and J. R. Li, *Sep. Purif. Technol.*, 2023, **304**, 122213.
11 P. Pinacho, M. M. Quesada-Moreno and M. Schnell, *J. Chem. Phys.*, 2023, **159**, 194305.
12 A. M. Chánique, N. Dimos, I. Drienovská, E. Calderini, M. P. Pantín, C. P. O. Helmer, M. Hofer, V. Sieber, L. P. Parra, B. Loll and R. Kourist, *ChemCatChem*, 2021, **13**, 2262.
13 S. Liu, Y. Long, S. Yu, D. Zhang, Q. Yang, Z. Ci, M. Cui, Y. Zhang, J. Wan, D. Li, A. Shi, N. Li, M. Yang and J. Lin, *Pharmacol. Res.*, 2021, **169**, 105627.
14 Y. Wang, T. Gao, Y. Lu, Y. Wang, Q. Cao and W. Fang, *Green Energy Environ.*, 2022, **7**, 275–287.
15 S. Y. Zhao, Y. S. Xiao, L. F. Yan, H. D. Zheng, F. W. Zhang, and B. Wu, *Chinese Pat.*, CN118255648, 2024.
16 H. D. Zheng, Z. Wang, Y. S. Xiao, L. F. Yan, F. W. Zhang, L. Chen, J. J. Chen, Y. S. Wang, and Z. Y. Yan, *Chinese Pat.*, CN117843449 A, 2024.
17 E. Soszka, M. Jędrzejczyk, C. Lefèvre, D. Ihiawakrim, N. Keller and A. M. Ruppert, *Catal. Sci. Technol.*, 2022, **12**, 5802–5813.
18 X. Rong, J. Yang, S. Liu, Y. Lan and Q. Liu, *CCS Chem.*, 2023, **5**, 1293–1300.
19 S. Chakrabortty, B. de Bruin and J. G. de Vries, *Angew. Chem., Int. Ed.*, 2024, **6**, e202315773.
20 C. Nguyen-Huy, H. Lee, J. Lee, J. H. Kwak and K. An, *Appl. Catal., A*, 2019, **571**, 118–126.
21 H. Zhao, X. Liao, H. Cui, M. Zhu, F. Hao, W. Xiong, H. Luo, Y. Lv and P. Liu, *Fuel*, 2023, **351**, 128887.
22 E. Soszka, M. Jędrzejczyk, N. Keller and A. M. Ruppert, *Fuel*, 2023, **332**, 126118.
23 Z. Huang, K. J. Barnett, J. P. Chada, Z. J. Brentzel, Z. Xu, J. A. Dumesic and G. W. Huber, *ACS Catal.*, 2017, **7**, 8429–8440.
24 X. He, Z. Hu, Q. Zou, J. Yang, R. Guo and L. Wu, *RSC Adv.*, 2023, **13**, 8901–8914.
25 D. Li, S. Zhang, Z. Mao, M. Liu, K. Hu, D. Zhao, D. Qv, L. Zhou and T. Shi, *RSC Adv.*, 2025, **15**, 9461–9466.